Quantitative textural analysis of packings of elongate crystals

John F. Rudge · Marian B. Holness · Graham C. Smith

February 18, 2008

Abstract

The spatial distribution of grains in a solidifying igneous rock controls the physical properties of the crystal mush, and is in turn controlled by the rate of crystal growth and accumulation. A predominant non-spherical habit for igneous minerals brings into question the use of spherical particles in reference packings used for quantification of spatial distribution. Furthermore, variations of crystal clustering/ordering with length scale require spatial statistics which take into account the distribution of particles beyond nearest neighbours. Using random close packings of spherocylinders we demonstrate the importance of aspect ratio for the aggregation index (usually known as R) and show that packings of spherical particles have more structure than packings of rods. The spatial distribution functions demonstrate that the plagioclase grains in the colonnade from the Holyoke basalt are clustered on a length scale of 0.5 mm. Understanding the controls on grain spatial distribution in igneous rocks will depend on application of these techniques to well-understood environments.

Keywords cumulates · textural analysis · spatial statistics · point patterns · random packing

Introduction

The spatial distribution of crystals in a solidifying plutonic rock exerts a major control on the distribution and connectivity of residual liquid, with consequences for physical properties such as permeability and rock rheology. The spatial distribution itself is a complex function of the mechanism of crystal accumulation (whether the crystals grew in situ in the thermal boundary layers of a magma chamber (Campbell 1978; Maaløe 1987; Marsh 1996), or whether they accumulated from gravity-driven crystal-rich slurries falling off the chamber roof and floor (Irvine 1987; Tepley and Davidson 2003; Wager et al. 1960) and the extent of deformation by compaction (McKenzie 1984; Shirley 1986) or flow (McBirney and Nicolas 1997). Furthermore, empirical studies have demonstrated that the initial porosity and structure of a crystal mush are highly sensitive to the rate at which the crystals accumulate (Blumenfeld et al. 2005), with immediate implications for the rheology and mass transport properties of the crystal mush on the boundaries of an open-system magma chamber in which periodic replenishment and discharge affected

J. F. Rudge (✉)
Bullard Laboratories, Department of Earth Sciences, Madingley Rise, Madingley Road, Cambridge CB3 0EZ, UK *and* Institute of Theoretical Geophysics, Department of Applied Mathematics and Theoretical Physics, Centre for Mathematical Sciences, Wilberforce Road, Cambridge CB3 0WA, UK.
E-mail: rudge@esc.cam.ac.uk. Tel: +44-1223-337176. Fax: +44-1223-360779.

M. B. Holness · G. C. Smith
Department of Earth Sciences, Downing Street, Cambridge, CB2 3EQ, UK.

the crystallisation rate. The complexity of the interplay between external controls and the architecture of the crystal mush is further illustrated by the control of crystal growth rates on grain shape, with rapid growth (for example, during degassing episodes in hydrous magmas) resulting in elongate or branching crystals (Donaldson 1976; Dunbar et al. 1995; Swanson and Fenn 1986). The packing and spatial distribution characteristics of such crystals will be different to those of rounded crystals of the same mineral formed during episodes of slower growth.

The first step towards understanding how these different processes affect rock rheology and the architecture of a crystal mush is an appropriate quantification of the spatial distribution of the component grains, which can then be used to compare different types of crystal mush. Quantifying spatial structure is usually done by looking at the point pattern statistics of grain centres in 2D thin sections (e.g. Carlson 1989; Jerram and Cheadle 2000; Jerram et al. 1996, 2003; Kretz 1966, 1969, 2006; Mock et al. 2003), or in 3D data (Hirsch et al. 2000; Ketcham et al. 2005). Such statistics can help quantify the complex clustering and ordering patterns that occur in a rock. To put these statistics into context, comparison has been made with reference textures based on numerical, experimental, and natural packings of spherical particles (Hirsch et al. 2000; Jerram and Cheadle 2000; Jerram et al. 1996, 2003; Ketcham et al. 2005). Sphere models have been used to study grain size variation, overgrowth and mechanical compaction in igneous rocks (Jerram et al. 1996), and crystal nucleation and growth in metamorphic rocks (Hirsch et al. 2000).

While reference textures based on spheres are appropriate for minerals such as olivine which generally forms equant, sub-rounded grains, they are not representative of microstructures formed in magmas in which the dominant phenocrysts are tabular or elongate such as plagioclase-dominated mafic rocks or for olivine-phyric rocks in which crystal growth forms are dendritic (e.g. O'Driscoll et al. 2007). Furthermore, spheres are exceptional in their packing behaviour, compared with more general shapes (Weitz 2004). Recently, there has been great interest in the random packing of non-spherical particles, such as ellipsoids (Donev et al. 2004), rods (Williams and Philipse 2003), and disks (Wouterse et al. 2007), providing us with an opportunity to expand our understanding of the interplay between particle packings, the physical behaviour of a crystal mush and the external physical controls on crystallisation using more realistic particle shapes. In this contribution we present the results of a preliminary exploration of the consequences of shape, specifically aspect ratio of rod-like particles, on the spatial distribution of grains and show how the grain distribution can be quantified. Due to the simplicity of textural analysis using thin sections, we focus on the quantitative analysis of randomly oriented 2D slices through a 3D crystal accumulation, although it should be noted that all the techniques described here have 3D analogues.

The paper is organised as follows. First, we describe various point pattern statistics for analysing textures: the aggregation index ("R"), Ripley's K function, pair correlation function, and mark correlation function; and discuss the importance of edge effects. An alternative to point pattern statistics, the autocorrelation, is then described. Numerical simulations of random packings of rods are discussed, and the various spatial statistics are applied to planar sections through the packings. We then explore clustered textures, illustrated with a natural example of a clustered texture from the colonnade of the Holyoke flood basalt. Finally, we discuss the relationship between 2D and 3D statistics.

Statistical methods for quantitative textural analysis

Point pattern statistics

Much information is recorded in the spatial distribution of centroids of grains observed in thin section, i.e. a point pattern. There are a wide range of statistical techniques for analysing such point patterns (the theory underpinning the generation of these patterns generally refers to point processes). Detailed reviews of these techniques can be found in Dixon (2002a,b); Mattfeldt (2005); Stoyan and Penttinen (2000). Many software packages are available for performing point pattern analysis: we used the freely available "spatstat" package (Baddeley and Turner 2005; R Development Core Team 2007).

At first order, a point pattern can be characterised by its intensity λ, which is defined as the number of points per unit area. Here we focus on the second order statistics which describe how the points are distributed relative to each other and can be used to determine if points are clustered (occurring close to each other) or ordered (repelled from each other). There are several popular second order statistics:

The aggregation index ("R")

The main statistic used by petrologists is the aggregation index R of Clark and Evans (1954) (also known as the ordering index). Its use to describe rock textures was pioneered by Kretz (1966, 1969), and it has since been used by many other authors (e.g. Boorman et al. 2004; Carlson 1989; Denison et al. 1997; Higgins 2006; Jerram et al. 1996, 2003; Kretz 2006). It is defined by

$$R = \frac{r_A}{r_E}, \tag{1}$$

where r_A is the mean of the distances separating points from their nearest neighbours, and r_E is the expected value of r_A for complete spatial randomness. r_E is given by

$$r_E = \frac{1}{2\sqrt{\lambda}}, \tag{2}$$

where λ is the intensity.

By definition, $R = 1$ for complete spatial randomness. If the points are clustered, the distance to nearest neighbours is shorter than that expected for complete spatial randomness and $R < 1$. Conversely, if points are ordered (with points further away than expected for spatial randomness) $R > 1$.

Fig. 1 shows four examples of 2D point patterns, with their R values. These were generated using models built into the "spatstat" package and give examples of: a) complete spatial randomness, b) clustering, c) ordering, and d) clustering and ordering on different scales. The aggregation index R clearly distinguishes between the random, the clustered, and the ordered patterns in Fig. 1a-c, but does not distinguish between complete spatial randomness (Fig. 1a) and the case with both clustering and ordering (Fig. 1d), since $R = 1.00$ in both cases. Fig. 1d demonstrates a key shortcoming of the aggregation index R: it cannot distinguish between clustering and ordering that occurs on different scales. R is "short-sighted" and cannot take into account behaviour further away than the nearest neighbour.

Fig. 1b shows an example generated by a Neyman-Scott cluster process. Instead of placing individual points randomly on the plane, the Neyman-Scott process places clusters of points randomly with a given cluster diameter and intensity. In Fig. 1b the cluster diameter was chosen to be 0.09. Fig. 1c is an example of a Strauss hard core process, in

which individual points are placed at random except they are not permitted to come closer to each other than a certain specified distance, known as a "hard core" distance (here a distance of 0.025 was chosen). The points can be thought of as disks in the plane with these radii that are not allowed to overlap. The presence of a hard core mimics the effect of finite grain size in a real rock: grain centres in a real rock cannot approach each other closer than their own diameter. Fig. 1d is a combination of the two above processes in which a Neyman-Scott process with a cluster diameter of 0.075 was "thinned" by removal of points closer than $r = 0.015$. Of all four example patterns, Fig. 1d is the closest to a real rock texture as it has clustering on a large scale in addition to the hard core (see later discussion of the Holyoke colonnade).

In order to quantify the complex ordering and clustering structure that occurs on multiple scales in a real rock we require a more sophisticated descriptor than R. This can be achieved using a function rather than an index, since functions can provide information about clustering and ordering on a variety of scales. We focus on Ripley's K function, the pair correlation function, and the mark correlation function. These functions have thus far been used by only a few authors in petrology, all interested in quantifying porphyroblast distribution in 3D in metamorphic rocks (Daniel and Spear 1999; Hirsch 2008; Hirsch et al. 2000; Ketcham et al. 2005; Raeburn 1996). The functions are very useful and straightforward to calculate.

Ripley's K function

Ripley's K function (Ripley 1976, 1977) is defined by

$$K(r) = \frac{\mathrm{E}\,(\text{number of extra points within radius } r \text{ of a randomly chosen point})}{\lambda}, \qquad (3)$$

where E denotes expectation. For complete spatial randomness, $K(r) = \pi r^2$. For convenience, Ripley's K function is usually plotted in the transformed form

$$L(r) = \sqrt{\frac{K(r)}{\pi}}, \qquad (4)$$

where $L(r) = r$ for complete spatial randomness. Note that alternative transformed forms are also popular, such as $\tilde{L}(r) = L(r) - r$.

Fig. 1 shows plots of $L(r)$ for the four example point patterns. The dashed line shows the behaviour expected for complete spatial randomness. Regions below the line indicate ordering of points, while those above denote clustering. The complete spatial randomness pattern we generated (Fig. 1a) shows no appreciable difference from the theoretical behaviour. The clustered pattern (Fig. 1b) lies above the line, while the ordered patten (Fig. 1c) falls below the line, as expected. The presence of the hard core in the ordered pattern is clearly visible in the $L(r)$ plot (Fig. 1c): there are no points closer than a distance of 0.025 and so $L(r)$ is zero for $r < 0.025$. Finally, $L(r)$ for the combined pattern (Fig. 1d) demonstrates both features: there is a hard core at small scales, followed by clustering at a larger scale.

Pair correlation function

An alternative, and sometimes clearer, representation of the information in Ripley's K function is the pair correlation function (or radial distribution function) $g(r)$, defined by

$$g(r) = \frac{1}{2\pi r}\frac{\mathrm{d}K(r)}{\mathrm{d}r}, \qquad (5)$$

where $g(r) = 1$ for complete spatial randomness. $g(r)$ determines how likely an interpoint distance of r is: if $g(r) > 1$ then it is more frequent than complete spatial randomness, if $g(r) < 1$ then it is less frequent than complete spatial randomness. The difference between Ripley's $K(r)$ and the pair correlation function, $g(r)$ (Fig. 1) is essentially the difference between a cumulative distribution function and a probability density function, where $g(r)$ is the probability density function for interpoint distances, appropriately normalised.

Fig. 1 shows plots of $g(r)$ for the four example point patterns. These are obtained by smoothing over a chosen length scale (analogous to the choice of bin size in a histogram, a technique known formally as kernel density estimation). The simulation of complete spatial randomness again shows no appreciable difference from that expected theoretically (except perhaps at small scales, but this is an artifact of small sample size). For the clustered pattern (Fig. 1b), $g(r)$ is initially much greater than 1, and decreases with increasing r until around $r = 0.09$ where it is then flat, lying on the dotted line $g(r) = 1$. $r = 0.09$ is a length scale characterising the clustering: until $r = 0.09$ interpoint distances are more common than they would be for complete spatial randomness. In this particular example, the characterstic length scale reflects the average size of clusters in the point pattern, which were chosen to have a diameter of 0.09.

The pair correlation for the ordered pattern (Fig. 1c) is zero for $r < 0.025$, but increases abruptly to 1 for $r = 0.025$, again demonstrating the hard core effect. Note that the sharp jump in gradient in the $L(r)$ plot has been smoothed out in the $g(r)$ plot, as a result of kernel density estimation. $g(r)$ for the combined clustered and ordered pattern (Fig. 1d) again shows both features: there is a small-scale hard core up to $r = 0.015$, followed by clustering up to a length scale of $r = 0.075$.

It should be noted that two point patterns can have the same pair correlation function whilst having quite different structures. For example, a pattern of isolated clusters can have the same pair correlation function as a pattern of linked chains. As such, the interpretion of pair correlation length scales requires some care, as the length scales will relate to different aspects of different patterns e.g. the clustering length scale could relate to the size of isolated clusters or to the spacing between chains. Despite this limitation, the pair correlation function still provides a useful summary of the point pattern and the characteristic length scales for clustering and ordering.

Mark correlation function

There is much more information in a thin section than simply the location of the centroids: the areas, orientations, long and short axes, etc. can also be calculated for each grain cross-section. One way of including such information in the point pattern statistics is to consider a marked point pattern. This is a point pattern in which each point has an associated numerical value (a mark). For example, the marks could be the effective radius of each grain cross-section ($\sqrt{\text{area}/\pi}$). The correlation of these marks can be expressed in terms of the mark correlation function, which depends on the interpoint distance r. The mark correlation function is defined in terms of a suitable test function $h(m_1, m_2)$ of two marks. A typical choice is the product

$$h(m_1, m_2) = m_1 m_2. \tag{6}$$

The mark correlation function is loosely defined by

$$m(r) = \frac{\mathrm{E}(h(m_1, m_2))}{\Lambda} \tag{7}$$

where m_1 and m_2 are marks separated by a distance r, E denotes expectation, and Λ is a normalisation such that $m(r) \equiv 1$ if the marks were independently distributed amongst the points. For the function in (6), $\Lambda = \overline{m}^2$ where $\overline{m}$ is the mean mark. Values of $m(r) \neq 1$ indicate some degree of correlation. For example, for thin sections it is expected that close pairs of points will correspond to small grains adjacent to other small grains and thus we expect $m(r) < 1$ at small scales for the radii mark correlation function. Note that, unlike the pair correlation function and Ripley's L function, the mark correlation function does not directly describe the clustering or ordering of the point pattern.

The mark correlation function using particle radius as the mark is sensitive to interactions due to crystal size. It is therefore useful in studies of the relative rates of growth of adjacent crystals in metamorphic rocks (i.e. the size isolation effect for porphyroblast growth (Hirsch et al. 2000) for which the radii mark correlation coefficient falls below unity at scales over which crystal growth is significantly retarded by diffusion), studies of competing crystals growing in situ from a liquid, or to the extent of mixing of different sized crystals in the context of a cumulate.

Ripley's L function, the pair correlation function, and the mark correlation function are most effectively used in combination with each other: A notable example of this is that the part of the clustering or ordering of a point pattern due to crystal size interactions can be distinguished from that due to other factors by comparing the pair correlation with the radii mark correlation.

Alternative statistics

An alternative method for studying the clustering and ordering of 2D point patterns of centroids was proposed by Jerram and Cheadle (2000). This method was based on cluster analysis, which has a very different aim to the spatial statistics described above. Cluster analysis is primarily a classification technique, and assigns points to groups based on their closeness to each other. It is particularly useful for identifying well separated groups of points. By contrast, Ripley's K function and the pair correlation function describe the overall clustering or ordering of a point pattern, rather than identify individual clusters. As such, we believe the functions discussed above provide a better description of the overall texture. An earlier study by Jerram et al. (1996) studied overall clustering and ordering on different length scales using inter-point distances and a technique called "pair analysis". This technique is closely related to, but different from, the pair correlation function used here.

There are two subtle assumptions that are implicit in the spatial statistics used here. Note that $L(r)$, $g(r)$ and $m(r)$ are functions of distance r alone, and thus there is an implicit assumption of isotropy (no preferred direction in the texture). The random packings we discuss are isotropic, but a real rock texture may not be. A second implicit assumption is stationarity (or homogeneity): loosely, that the point pattern is invariant to translation in a statistical sense. Only if a point pattern is assumed to be stationary does it make sense to describe it by a single intensity λ rather than an intensity $\lambda(\mathbf{x})$ as a function of position. There are generalisations of the point pattern statistics that do not assume isotropy and stationarity. For example, the reduced second moment measure (Stoyan et al. 1995; Stoyan and Stoyan 1994) generalises Ripley's K function to use a vector displacement rather than distance, and thus does not assume isotropy. Such generalised statistics and more can be found in "spatstat" (Baddeley and Turner 2005).

Edge effects

In practice, point patterns are only observed over a finite region. When studying a point pattern, it is therefore important to specify not only the locations of the points, but also the window in which the points are observed. It is important to understand, and correct for, the edge effects that arise from having a limited observation window.

Edge effects arise in two main ways in the point pattern analysis of thin sections. The first edge effect arises in going from the 2D slice to the point pattern. On the edge of the window there may be incomplete grains where part of the grain lies outside the window. However, the centroid of this incomplete grain may lie within the window. Hence, if incomplete grains are omitted, then the point pattern will have fewer points near the edge than it should, and all the statistics will be biased (e.g. Baddeley and Jensen 2004, Ch. 3).

An example of this first kind of edge effect is shown in Fig. 2. Here a slice through the experimental random close packing of spheres of Finney (1970) has been taken, following the method of Jerram et al. (1996). The slice contains complete grains only. If the point pattern of centroids is chosen to have the same observation window as the original 2D slice, then there is a notable lack of points near the edge of the domain (solid box, middle figure). This leads to an underestimate of the intensity of the point pattern, and thus to an underestimate of the aggregation index R (since r_E will be overestimated). The simplest way of correcting for this bias is to reduce the size of the observation window appropriately ('minus sampling'), and ignore any points outside the new window (solid box, right figure). The intensity of the point pattern is then estimated by the number of points per unit area inside the new window, and r_E follows from equation 2.

The second kind of edge effect is common to all point pattern analyses. When calculating statistics involving neighbouring points, a bias is introduced because nothing is known about points outside the observation window. For example, it may be that the true nearest neighbour of a point lies outside the observation window, and so a naive calculation of r_A will be an overestimate, and thus R will be overestimated. The simplest correction for this is to introduce a "guard region" or "buffer zone" (Fig. 2, dashed box, right figure) near the edge of the observation window where nearest neighbour distances are not calculated, but the points are available as neighbours for the points in the inner region (Clark and Evans 1954). The buffer zone should be large enough so that the nearest neighbours of points in the inner region can always be found either in the inner region or in the buffer zone. Choosing the size of the buffer zone optimally is difficult: if it is too large, valuable data is discarded; if too small, edge effects will remain (Pommerening and Stoyan 2006). It should be noted that the buffer zone is ignored in the calculation of r_E, as there is no bias in estimating the intensity using the whole observation window (solid box, right figure).

The particular example in Fig. 2 shows that edge effects can be significant. For the slice shown, a naive calculation leads to an aggregation index $R = 1.64$. When the first edge effect is corrected, this rises to 1.74, and is reduced only slightly by correcting for the second effect, to 1.73. On averaging the results from 1000 random slices, the new estimate for the Finney (1970) sphere packing is $R = 1.73$, 5% larger than $R = 1.65$ originally quoted by Jerram et al. (1996).

All the statistics described in the previous section have been edge corrected using routines built in to the "spatstat" package (Baddeley and Turner 2005), and this should usually be done. The main disadvantage of edge correction is that the variability of the result will increase if points are neglected (as in "minus sampling"), resulting in less representative values of the statistical measures. This may be a problem if there are only

very few points in the sample.

Autocorrelation

As an alternative to point pattern statistics, there are a number of image processing techniques that directly yield information about spatial structure from raw 2D slice images. One of the simplest techniques is the calculation of the autocorrelation function $C(\mathbf{r})$ (also known as the two-point correlation function (Berryman and Blair 1986; Blair et al. 1996) or the covariance (Stoyan et al. 1995). $C(\mathbf{r})$ is defined by

$$C(\mathbf{r}) = \langle f(\mathbf{x}) f(\mathbf{x}+\mathbf{r}) \rangle \tag{8}$$

where $\mathbf{r}$ is a given vector, and $\langle \cdot \rangle$ denotes an average over all points $\mathbf{x}$ in the image. $f(\mathbf{x})$ is an indicator function, defined by

$$f(\mathbf{x}) = \begin{cases} 1 & \text{if } \mathbf{x} \text{ is in a grain,} \\ 0 & \text{otherwise.} \end{cases} \tag{9}$$

The autocorrelation measures how well an image matches a spatially shifted version of itself. Autocorrelations are efficiently calculated using Fast Fourier Transforms, and are available in standard image processing packages such as ImageJ (Rasband 1997-2007). For isotropic textures, $C(\mathbf{r}) = C(r)$, a function of distance alone (indeed, examining whether $C(\mathbf{r})$ satisfies this condition is a good way of identifying anisotropy). The autocorrelation function satisfies

$$C(0) = 1 - \phi, \tag{10}$$

$$C(r) \to (1-\phi)^2 \quad \text{as} \quad r \to \infty, \tag{11}$$

where ϕ is the porosity and $1-\phi$ is the volume fraction of grains. As such, some authors work with a rescaled version (Morishita 1998; Morishita and Obata 1995)

$$\sigma(r) = \frac{C(r) - (1-\phi)^2}{\phi\,(1-\phi)}, \tag{12}$$

which satisfies

$$\sigma(0) = 1, \tag{13}$$

$$\sigma(r) \to 0 \quad \text{as} \quad r \to \infty. \tag{14}$$

For a closer comparison with what is typically found in the packing literature, we use the unscaled version.

The autocorrelation function provides a compact description of the microstructure of the packing. The length scale over which it decays can provide insight into the grain scale and length scale of clustering. It can also be used to calculate the specific surface area of the microstructure, which is proportional to $C'(0)$ (Berryman and Blair 1986). However, unlike point pattern statistics, the autocorrelation does not identify individual grains: it simply deals with the group of grains as a whole. It should be noted that there are other techniques that have been used for analysing 2D slice images (e.g. Gaillot et al. 1997), but for simplicity we consider only the autocorrelation.

Random packings of rods

In order to develop an understanding of real rock microstructures, comparison must be made between natural samples and reference textures. There are many different ways to generate a random packing of particles, and the packing that results is highly dependent on the scheme used (Stoyan 2002). We concentrate on random close packing (more formally known as maximally random jammed packing (Torquato et al. 2000)) which is loosely defined as the maximum density state for a random collection of particles. A random close packing of identical spheres has a porosity $\phi = 0.36$. Remarkably, particles with a slightly larger aspect ratio can pack more densely than spheres, with a minimum porosity of 0.30 achieved for rods (Williams and Philipse 2003) and $\phi = 0.26$ for ellipsoids (Donev et al. 2004). This improvement in packing density may be due to the extra rotational degrees of freedom associated with non-spherical particles (a sphere is invariant under any rotation, a rod is not) (Weitz 2004).

Here we use identical rods as a simple analogue for elongate crystals. The rods are actually spherocylinders, which are cylinders with spherical caps, specified by the diameter D and length L of the cylinder (Fig. 3), described by an aspect ratio $\alpha = L/D$. Note that the true aspect ratio of spherocylinders is $1 + \alpha$, and that $\alpha = 0$ corresponds to a sphere. We use the rod packings generated by Williams and Philipse (2003) who performed numerical simulations using a mechanical contraction algorithm inside a periodic box to generate 3-dimensional packings. We re-examine their rod packings in thin section by slicing through the 3D packings at random orientations. Fig. 4 shows 3D plots of the spherocylinder packings along with a representive thin section for different values of α.

Fig. 5 shows the variation in porosity with α found by Williams and Philipse (2003). As α increases, the porosity decreases down to a minimum around $\alpha = 0.5$, after which it monotonically increases. For large α, the porosity is thought to increase as $\phi \sim 1 - 5.4/\alpha$ (Philipse 1996a,b). This result has important implications for the solidification of igneous rocks as the initial porosity of a crystal mush on a chamber floor, accumulating by gravitational settling, will be highly sensitive to grain shape (assuming that no preferred orientation of elongate grains develops during either the settling process or subsequent compaction). Comparison of cumulates thought to have formed by gravitational settling, and with only insignificant, post-accumulation over-growth of the cumulus grains, demonstrate this first-order control on mush architecture. The initial porosity of a cumulate formed predominantly of rounded equant olivine grains, such as that common in the peridotite horizons of the Rum Layered Suite (Fig. 6a), will generally be much less than that in a cumulate formed of elongate crystals with large aspect ratio ($\gtrsim 3.5 : 1$, Fig. 6b), if orientation effects and early clustering are ignored.

Analysis of rod packings

The spatial statistics described earlier were calculated from 1000 random slices through each of the rod packings and are shown in Figs. 7, 8 and 9. To generate the random slices, the packings were first rotated or reflected by one of the 48 symmetries of the cube. A high resolution digital slice (4096×4096 pixels) was then taken at a random height uniformly distributed in the z-direction. The packings are periodic, and this was exploited in calculating the spatial statistics of the 2D slices.

R versus porosity

The aggregation index R compares the mean nearest neighbour distance to that of complete spatial randomness. However, complete spatial randomness is not a good reference for point patterns created by centroids of real particles. Due to the finite grain size, two centroids cannot approach closely, and this produces larger than expected nearest neighbour distances. This discrepancy increases with decreasing porosity and is also affected by a spread in the population of grain diameters. To avoid these problems, Jerram et al. (1996) proposed that R for centroids should be compared to a value generated from a reference texture.

The reference textures Jerram et al. (1996) proposed were based on random packings of monodisperse spheres (i.e. spheres of a single size). The general idea was to compare a given R to that produced by a random packing of spheres with equal porosity. This was expressed in terms of the R against porosity plot (Fig. 7). Jerram et al. (1996) proposed a reference line for this plot called the "Random Sphere Distribution Line (RSDL)". All but one of the points on the RSDL were generated by numerical simulations of sphere packings with various porosities, by random sequential addition of spheres. The final point on the RSDL (the one with lowest porosity $\phi = 0.36$) was that of the experimental random close packing of spheres by Finney (1970). If a sample lay below the RSDL its grains were said to be clustered; if above, ordered (Jerram et al. 1996).

An important first observation is that the sphere packing used here ($\phi = 0.36$, $R = 1.73$) does not lie on the RSDL proposed by Jerram et al. (1996). The discrepancy is probably caused by edge effects. When Jerram's analysis of the Finney packing (top end of the RSDL) is edge corrected the value goes from $R = 1.65$ to $R = 1.73$ and is then in very close agreement with the numerical simulation used here. It seems likely that all R values on the RSDL are slightly biased, and need reanalysing for edge effects.

The value of R calculated for the rod packings are also shown in Fig. 7. R monotonically decreases with α (Fig. 8). As porosity does not behave in the same way (Fig. 5), the rod packing trend in Fig. 7 is curved. Shape seems to plays an important role in determining R: for example, $\alpha = 0.0$ and $\alpha = 2.0$ have very similar porosities, but their R is quite different: $R = 1.73$, and $R = 1.58$ respectively. Jerram et al. (1996) discusses in more detail other factors that influence R, such as overgrowth, compaction and polydispersivity.

It should be noted that all the rod packings shown in Fig. 7 are random close packings, and thus form touching frameworks. This is not the case with the points on the RSDL, as only the Finney packing is a random close packing. For large porosities the points on the RSDL do not come from touching frameworks, and this led Jerram et al. (2003) to propose that the R against porosity plot may provide a way to distinguish touching and non-touching frameworks. However, in general, whether crystals form a touching framework or not will depend in a complicated way on grain shape, grain size, and how the grains are packed. As such, a simple classification of touching and non-touching frameworks by the R versus porosity plot seems unlikely.

Correlation functions

More detailed information about the packings can be gained by looking at the various functions described earlier. Fig. 9 plots Ripley's L function, the pair correlation function, the radii mark correlation function, and the autocorrelation for 2D slices through the rod packings shown in Fig. 4. The units of distance have been chosen so that the diameter D of the spheres and rods is 1.

For all of the packings, all of the point pattern statistics ($L(r)$, $g(r)$ and $m(r)$) show

clear evidence of small scale repulsion, as is expected from the finite size of the rods: all the curves are below the dashed lines for small values of r. The length scale of the small scale repulsion is near 1 in each case, which corresponds to the diameter D of the spheres and rods.

One striking observation is the amount of structure present in a random packing of monodisperse spheres (top row, Fig. 9). An alternating pattern of clustering and ordering of the point pattern on different scales is clearly visible. This structure is clearest in the pair correlation function. An interpoint distance of 1 is very common (the diameter of the spheres), and this is reflected by a sharp peak. Closer distances are much less common, as is expected from volume exclusion effects. However, it should be noted that the slices through the sphere packing do not have a hard core, unlike the examples shown in Fig. 1c-d: both $L(r)$ and $g(r)$ are non-zero for all $r > 0$. This is understandable, for while two sphere centres cannot approach each other closer than their diameters, the centroids of two sphere cross-sections can. As such, it is merely less likely that short interpoint distances are found, not impossible, and this is sometimes referred to as "soft core" behaviour.

As α is increased, a lot of the alternating structure vanishes due to the broken symmetry. A hard core appears to develop, with very few points occurring at less than a distance of 1. This is also understandable, as interpoint distances less than 1 can only occur in thin section when the end of a rod is sliced. As the rods get longer, this scenario becomes less likely. The L function and pair correlation function for $\alpha = 40.0$ somewhat resembles the hard core ordered pattern in Fig. 1c.

There is no variation in grain size in any of the packings. However, there is a variation in the size of grain cross-sections ("apparent grain size") in the 2D slices, and the 2D mark correlation function is sensitive to this. Short interpoint distances are associated with small grain cross-sections due to slicing the ends of rods. Hence the mark correlation function is below the dashed line for small interpoint distances, and increases with increasing r until around $r = 1$ in each case, corresponding to the diameter D of the rods and spheres. As with the pair correlation function, there is some additional oscillating structure visible in the mark correlation function for small α, but this diminishes as α increases.

For all the packings, the autocorrelation $C(r)$ dies away over a length scale of 1 in keeping with 1 being the diameter of the rods. The sphere packing again shows the most structure, with oscillations above and below the long range value. These oscillations again diminish as α increases.

Clustered textures

Correlation functions can be used to detect the clustering of grains, and the length scale over which clustering takes place. As an example, Figs. 10 and 11 show two artificially clustered textures, where again the diameter D of the rods and spheres is 1. In Fig. 10 the random sphere packing has been altered by randomly removing groups of spheres to leave a "swiss-cheese" texture. The holes in the swiss-cheese texture were chosen to have a radius of 3.5. Fig. 10 should be compared to the first row of Fig. 9. The L function is now above the dotted line at large scales, indicative of clustering. The pair correlation has likewise been shifted so that interpoint distances for $r \lesssim 3.5$ are more common than they were, although the alternating structure remains. This identifies 3.5 as a characteristic length scale for the clustering, which is equal to the chosen diameter of the holes. The radii mark correlation function is unchanged: this is expected, since the radii mark correlation is only sensitive to the radii of points separated by a particular distance, not to how many points are separated by a particular distance. It is thus useful to compare the radii mark

correlation function with the pair correlation function to distinguish between crystal size interactions and overall clustering of the framework. In this case, apparent crystal size interactions are important on interpoint distances up to 1 (mark correlation), and overall clustering on interpoint distances up to 3.5 (pair correlation). The autocorrelation also hints at the different scales in the packing: there is a kink near 1, and the curve tails off near 3.5.

Fig. 11 shows a similar artificially clustered packing, this time for a rod packing with $\alpha = 10$, to be compared with the fourth row of Fig. 9, with a chosen hole diameter of 10. The effect of the clustering is easier to distinguish in this example, because there is less structure present in the original packing. Again $L(r)$ is above the dotted line at large scales. The pair correlation is above the line up to around $r = 10$, so that 10 is the characteristic length scale of the clustering, which again reflects the chosen diameter of the holes. Again, the radii mark correlation function is unchanged while the autocorrelation function has a noticeable kink near $r = 1$, again showing the presence of different scales in the packing.

The Holyoke colonnade

The 200m thick Holyoke flood basalt (Connecticut and Massachusetts, USA) is notable for the demonstration that plagioclase micro-crystals in experimentally-melted samples form a framework of chains of touching grains when the porosity is as high as 75% (Philpotts et al. 1998). The basalt flow comprises a quench-textured roof-crust (the entablature) while the texture in the upwards-crystallising floor zone (the colonnade) results from the recrystallisation of crystal-rich plumes fallen from the roof zone (Philpotts and Dickson 2000). The plagioclase crystals in the colonnade inherit the clustering formed early in the solidification history of the entablature (Jerram et al. 2003), with the chains separated by granular pyroxene aggregates which are recrystallised remnants of ophitic pyroxene-plagioclase clusters that nucleated within the spaces between the chains (Jerram et al. 2003; Philpotts and Dickson 2000).

Fig. 12 shows a line drawing of the plagioclase grains in a sample from the colonnade of the Holyoke flood basalt. The clustering of the plagioclase grains is clear in both the raw image and the statistics (Fig. 12). $R = 0.75$ for the point pattern, which indicates clustering regardless of which reference texture it is compared to. The pair correlation function shows ordering at length-scales below about 0.05 mm (an obvious consequence of finite grain size), and then clustering up to around 0.5 mm. The autocorrelation function similarly shows a characteristic length scale of 0.5 mm associated with the clustering. The mark correlation function indicates that crystal size interactions are only important on scales up to 0.15 mm. Unlike the packing examples, the Holyoke colonnade has a real variation in grain size and not just apparent grain size. Since the length scale for clustering of the point pattern (0.5 mm) is so different to that of crystal size interactions (0.15 mm), the crystals must be forming a clustered framework. The characteristic length scale of the clustering probably corresponds to the characteristic spacing between the plagioclase chains (c.f. Philpotts and Dickson 2000), in a similar way that the characteristic clustering length scales of Figs. 10 and 11 relate to hole size.

It is not entirely clear how to interpret the mark correlation function in the context of igneous textures. For metamorphic textures, the length scale for crystal size interactions found from the mark correlation function has been interpreted in terms of the distance over which diffusion controls crystal size (e.g Hirsch et al. 2000; Ketcham et al. 2005). This would be appropriate for the Holyoke colonnade if it were the case that the plagio-

clase grains had nucleated and grown in situ. However, consideration of the compositions of plagioclase grains within the clusters lead Philpotts et al. (1998) to suggest that the plagioclase crystals nucleated and remained freely suspended for some time before joining to form the chains by synneusis. Hence, crystal size interactions in igneous textures may depend on how different sizes of crystals mix. A better understanding is likely to come from combining the information in the mark correlation function with crystal size distribution data. Despite this current lack of understanding, the mark correlation function still provides an important constraint on the length scale over which crystal size interactions are important.

The relationship between 2D and 3D

All the analysis shown has been on 2D thin sections, but the statistical techniques can also be applied in 3D (e.g. Hirsch et al. 2000). Unfortunately, there are no general stereological relationships between 2D point pattern statistics of grain cross-sections and 3D statistics of grain centres. A key advantage of the autocorrelation over point pattern statistics is that it is the same in 3D as 2D, assuming the medium is isotropic. This is not to say that 2D point pattern statistics are not useful: indeed, as has been shown, 2D statistics provide a good description of the structure. Moreover, the 2D statistics are similar to the 3D statistics at larger scales (Stoyan et al. 1995). For example, the 3D pair correlation function of sphere centres for random sphere packing is shown in Fig. 13. Apart from near $r \leq 1$ the 3D pair correlation function is very similar to the 2D pair correlation shown in Fig. 9. The difference at small scales arises because while two sphere centres can never be less than a distance D apart, the centroids of two profiles can. For a more detailed discussion of the stereology of spatial statistics see Chapter 8 of Stoyan et al. (1995). 3D textural information is becoming more readily available (Jerram and Higgins 2007), and future studies should quantify spatial structure in terms of the 3D versions of the techniques. 3D pair correlation functions and autocorrelations are commonly quoted in the packing literature, and will provide a good source for comparison.

Conclusions

When studying the spatial distribution of grains in a rock it is important to compare with reference textures that have grains with a similar aspect ratio. Whilst packings of spheres should be an appropriate reference texture for materials with equant grains, materials with elongate grains are better compared to packings of rods. The statistical techniques discussed here, based on correlation functions, rather than on single indices such as R, show that sphere packings contain a great deal of structure that is not found in packings of more general shapes.

The rod packings we have used have notable shortcomings as a reference texture. The main disadvantage is that all the packings studied here comprise populations of identical particles (i.e. they are monodisperse). Real rocks contain crystals of a wide range of sizes, and this will play an important role in their packing behaviour. While there are some published studies of polydisperse packings of spheres (e.g. Bezrukov et al. 2001; Lochmann et al. 2006), there seem to be few corresponding studies of polydisperse packing of more general shapes. The polydisperse packings more representative of igneous rocks are likely to show less inherent structure than the monodisperse packings described here. Future reference textures need to be more random in the shape and size of their crystals, to better model real rocks.

A further drawback is that it is not clear how applicable random close packing is for igneous rocks. The reference textures we have used here all have the maximum density, and while this state undoubtedly is possible to achieve for e.g. a sandstone or oolitic limestone (Fig. 6c), the relatively small density difference between solid and liquid, together with the high viscosity of typical silicate liquids, means that gravitational settling may result in a much looser packing than our reference textures. A further complication is presented by in situ nucleation and growth of primocrystic phases in the cumulate mush. Such grains infill primary porosity but may not be easily distinguishable from the gravitationally accumulated grains. They may also nucleate and grow on pre-existing grains, inheriting a pre-determined crystal orientation.

The illustration of the information which can be extracted from a thin section of basalt using functions rather than indices to quantify grain distributions demonstrates not only that there is much information which can be extracted relatively easily, but also that we are in the very early stages of understanding what the information actually means. Although such sophisticated treatments have already been applied to metamorphic rocks (e.g. Hirsch et al. 2000) the case of igneous rocks, in which individual particles can move relative to each other in the early stages of solidification, is still unexplored territory. We are yet to begin to tease apart the importance of crystal accumulation rate on the extent and size of clusters in solidifying rocks (e.g. Blumenfeld et al. 2005), despite the importance of such an effect on the rheology of ascending magmas and the permeability and ease of compaction of cumulates. Application of the techniques outlined here to suites of rocks from different magmatic environments is the way forward.

Acknowledgements We are extremely grateful to Dougal Jerram, whose work was the inspiration for this study, for all his help: providing us with the co-ordinates of the Finney sphere packing, the co-ordinates of the RSDL, and the tracing of the Holyoke colonnade. We are also extremely grateful to Alan Wouterse and Albert Philipse for providing us with the co-ordinates of their spherocylinder packings. We thank Madeleine Humphreys and Rachel Sides for helpful discussions, and Dougal Jerram and Mike Cheadle for their constructive reviews. John Rudge was supported by a Junior Research Fellowship at Trinity College, Cambridge. Graham Smith was supported by a NERC studentship.

References

Aste T, Saadatfar M, Senden TJ (2005) Geometrical structure of disordered sphere packings. Phys Rev E 71:061302. doi:10.1103/PhysRevE.71.061302

Baddeley A, Jensen EBV (2004) Stereology for Statisticians. Chapman & Hall/CRC. ISBN-10-1584884053

Baddeley A, Turner R (2005) Spatstat: an R package for analyzing spatial point patterns. J Stat Soft 12:1–42. URL `www.jstatsoft.org`, ISSN 1548-7660

Berryman JG, Blair SC (1986) Use of digital image analysis to estimate fluid permeability of porous materials: Application of two-point correlation functions. J Appl Phys 60:1930–1938. doi:10.1063/1.337245

Bezrukov A, Stoyan D, Bargiel M (2001) Spatial statistics for simulated packings of spheres. Image Anal Stereol 20:203–206

Blair SC, Berge PA, Berryman JG (1996) Using two-point correlation functions to characterize microgeometry and estimate permeabilities of sandstones and porous glass. J Geophys Res 101:20359–20375. doi:10.1029/96JB00879

Blumenfeld R, Edwards SF, Ball RC (2005) Granular matter and the marginal rigidity state. J Phys: Condens Matter 17:S2481–S2487. doi:10.1088/0953-8984/17/24/007

Boorman S, Boudreau A, Kruger FJ (2004) The Lower Zone-Critical Zone transition of the Bushveld complex: a quantitative textural study. J Petrol 45:1209–1235. doi:10.1093/petrology/egh011

Campbell IH (1978) Some problems with the cumulus theory. Lithos 11:311–323. doi:10.1016/0024-4937(78)90038-5

Carlson WD (1989) The significance of intergranular diffusion to the mechanisms and kinetics of porphyroblast crystallization. Contrib Mineral Petrol 103:1–24. doi:10.1007/BF00371361

Clark PJ, Evans FC (1954) Distance to nearest neighbor as a measure of spatial relationships in populations. Ecology 35:445–453

Daniel CG, Spear FS (1999) The clustered nucleation and growth processes of garnet in regional metamorphic rocks from north-west Connecticut, USA. J Metamorphic Geol 17:503–520

Denison C, Carlson WD, Ketcham RA (1997) Three-dimensional quantitative textural analysis of metamorphic rocks using high-resolution computed X-ray tomography: Part I. Methods and techniques. J Metamorphic Geol 15:29–44. doi:10.1111/j.1525-1314.1997.00006.x

Dixon PM (2002a) Nearest neighbor methods. In: El-Shaarawi AH, Piegorsch WW (eds) Encyclopedia of Environmetrics. John Wiley & Sons. doi:10.1002/9780470057339.van007

Dixon PM (2002b) Ripley's K function. In: El-Shaarawi AH, Piegorsch WW (eds) Encyclopedia of Environmetrics. John Wiley & Sons. doi:10.1002/9780470057339.var046

Donaldson CH (1976) An experimental investigation of olivine morphology. Contrib Mineral Petrol 57:187–213. doi:10.1007/BF00405225

Donev A, Cisse I, Sachs D, Variano EA, Stillinger FH, Connelly R, Torquato S, Chaikin PM (2004) Improving the density of jammed disordered packings using ellipsoids. Science 303:990–993. doi:10.1126/science.1093010

Dunbar NW, Jacobs GK, Naney MT (1995) Crystallization processes in an artificial magma: variations in crystal shape, growth rate and composition with melt cooling history. Contrib Mineral Petrol 120:412–425. doi:10.1007/s004100050085

Finney JL (1970) Packings and the structure of simple liquids. I. The geometry of random close packing. Proc Roy Soc A 319:479–493

Gaillot P, Darrozes J, de Saint Blanquat M, Ouillon G (1997) The normalised optimised anisotropic wavelet coefficient (NOAWC) method: An image processing tool for multiscale analysis of rock fabric. Geophys Res Lett 24:1819–1822

Higgins MD (2006) Quantitative textural measurements in igneous and metamorphic petrology. Cambridge University Press. ISBN-13: 9780521847827 doi:10.2277/0521847826

Hirsch DM (2008) Controls on porphyroblast size along a regional metamorphic field gradient. Contrib Mineral Petrol in press. doi:10.1007/s00410-007-0248-y

Hirsch DM, Ketcham RA, Carlson WD (2000) An evaluation of spatial correlation functions in textural analysis of metamorphic rocks. Geol Mat Res 2:1–42

Irvine TN (1987) Layering and related structures in the Duke Island and Skaergaard intrusions: similarities, differences, and origins. In: Reidel D (ed) Origins of Igneous Layering. Dordrecht, pp 185–245

Jerram DA, Cheadle MJ (2000) On the cluster analysis of grains and crystals in rocks. Amer Mineral 85:47–67

Jerram DA, Cheadle MJ, Hunter RH, Elliott MT (1996) The spatial distribution of grains and crystals in rocks. Contrib Mineral Petrol 125:60–74. doi:10.1007/s004100050206

Jerram DA, Cheadle MJ, Philpotts AR (2003) Quantifying the building blocks of igneous rocks: are clustered crystal frameworks the foundation? J Petrol 44:2033–2051. doi:10.1093/petrology/egg069

Jerram DA, Higgins MD (2007) 3D analysis of rock textures: Quantifying igneous microstructures. Elements 3:239–245. doi:10.2113/gselements.3.4.239

Ketcham RA, Meth C, Hirsch DM, Carlson WD (2005) Improved methods for quantitative analysis of three-dimensional porphyroblastic textures. Geosphere 1:42–59. doi:10.1130/GES00002.1

Kretz R (1966) Grain-size distribution for certain metamorphic minerals in relation to nucleation and growth. J Geol 74:147–173

Kretz R (1969) On the spatial distribution of crystals in rocks. Lithos 2:39–65. doi:10.1016/S0024-4937(69)80005-8

Kretz R (2006) Shape, size, spatial distribution and composition of garnet crystals in highly deformed gneiss of the Otter Lake area, Québec, and a model for garnet crystallization. J Metamorphic Geol 24:431–449. doi:10.1111/j.1525-1314.2006.00647.x

Lochmann K, Oger L, Stoyan D (2006) Statistical analysis of random sphere packings with variable radius distribution. Solid State Sci 8:1397–1413. doi:10.1016/j.solidstatesciences.2006.07.011

Maaløe S (1987) The origin of rhythmic layering. Mineral Mag 42:337–345

Marsh BD (1996) Solidification fronts and magmatic evolution. Mineral Mag 60:5–40

Mattfeldt T (2005) Explorative statistical analysis of planar point processes in microscopy. J Microsc 220:131–139. doi:10.1111/j.1365-2818.2005.01521.x

McBirney AR, Nicolas A (1997) The Skaergaard layered series. Part II. Magmatic flow and dynamic layering. J Petrol 38:569–580

McKenzie D (1984) The generation and compaction of partially molten rock. J Petrol 25:713–765. doi:10.1093/petrology/25.3.713

Mock A, Jerram DA, Breitkreuz C (2003) Using quantitative textural analysis to understand the emplacement of shallow-level rhyolitic laccoliths–a case study from the Halle Volcanic Complex, Germany. J Petrol 44:833–849. doi:10.1093/petrology/44.5.833

Morishita R (1998) Statistical properties of ideal rock textures: Relationship between crystal size distribution and spatial correlation of minerals. Math Geol 30:409–434

Morishita R, Obata M (1995) A new statistical description of the spatial distribution of minerals in rocks. J Geol 103:232–240

O'Driscoll B, Donaldson CH, Troll VR, Jerram DA, Emeleus CH (2007) An origin for harrisitic and granular olivine in the Rum layered suite, NW Scotland: a crystal size distribution study. J Petrol 48:253–270. doi:10.1093/petrology/egl059

Philipse AP (1996a) The random contact equation and its implications for (colloidal) rods in packings, suspensions, and anisotropic powders. Langmuir 12:1127–1133. doi:10.1021/la950671o

Philipse AP (1996b) The random contact equation and its implications for (colloidal) rods in packings, suspensions, and anisotropic powders (correction). Langmuir 12:5971. doi:10.1021/la960869o

Philpotts AR, Dickson LD (2000) The formation of plagioclase chains during convective transfer in basaltic magma. Nature 406:59–61

Philpotts AR, Shi J, Brustman C (1998) Role of plagioclase crystal chains in the differentiation of partly crystallized basaltic magma. Nature 395:343–346. doi:10.1038/26404

Pommerening A, Stoyan D (2006) Edge-correction needs in estimating indices of spatial forest structure. Can J For Res 36:1723–1739. doi:10.1139/X06-060

R Development Core Team (2007) R: A Language and Environment for Statistical Computing. R Foundation for Statistical Computing, Vienna, Austria. URL `http://www.R-project.org`, ISBN 3-900051-07-0

Raeburn SP (1996) New methods in quantitative metamorphic petrology: 1. In situ determinations of iron valence in minerals; 2. The application of 3-D textural analysis to the study of crystallization kinetics. Ph.D. thesis, Pennsylvania State University

Rasband W (1997-2007) ImageJ. U. S. National Institutes of Health, Bethesda, Maryland, USA. URL http://rsb.info.nih.gov/ij/

Ripley BD (1976) The second-order analysis of stationary point processes. J Appl Prob 13:255–266

Ripley BD (1977) Modelling spatial patterns. J Roy Stat Soc B 39:172–192

Shirley DN (1986) Compaction of igneous cumulates. J Geol 94:795–809

Stoyan D (2002) Simulation and characterization of random systems of hard particles. Image Anal Stereol 21:S41–S48

Stoyan D, Kendall WS, Mecke J (1995) Stochastic geometry and its applications. J Wiley and Sons

Stoyan D, Penttinen A (2000) Recent applications of point process methods in forestry statistics. Statist Sci 15:61–78

Stoyan D, Stoyan H (1994) Fractals, random shapes and point fields: methods of geometrical statistics. J Wiley and Sons

Swanson SE, Fenn PM (1986) Quartz crystallisation in igneous rocks. Amer Mineral 71:331–342

Tepley FJI, Davidson JP (2003) Mineral-scale Sr-isotope constraints on magma evolution and chamber dynamics in the Rum layered intrusion, Scotland. Contrib Mineral Petrol 145:628–641. doi:10.1007/s00410-003-0481-y

Torquato S, Truskett TM, Debenedetti PG (2000) Is random close packing of spheres well defined? Phys Rev Lett 84:2064–2067. doi:10.1103/PhysRevLett.84.2064

Wager LR, Brown GM, Wadsworth WJ (1960) Types of igneous cumulates. J Petrol 1:73–85. doi:10.1093/petrology/1.1.73

Weitz DA (2004) Packing in the spheres. Science 303:968–969. doi:10.1126/science.1094581

Williams SR, Philipse AP (2003) Random packings of spheres and spherocylinders simulated by mechanical contraction. Phys Rev E 67:051301. doi:10.1103/PhysRevE.67.051301

Wouterse A, Philipse AP (2006) Geometrical cluster ensemble analysis of random sphere packings. J Chem Phys 125:194709. doi:10.1063/1.2390700

Wouterse A, Williams SR, Philipse AP (2007) Effect of particle shape on the density and microstructure of random packings. J Phys: Condens Matter (in press)

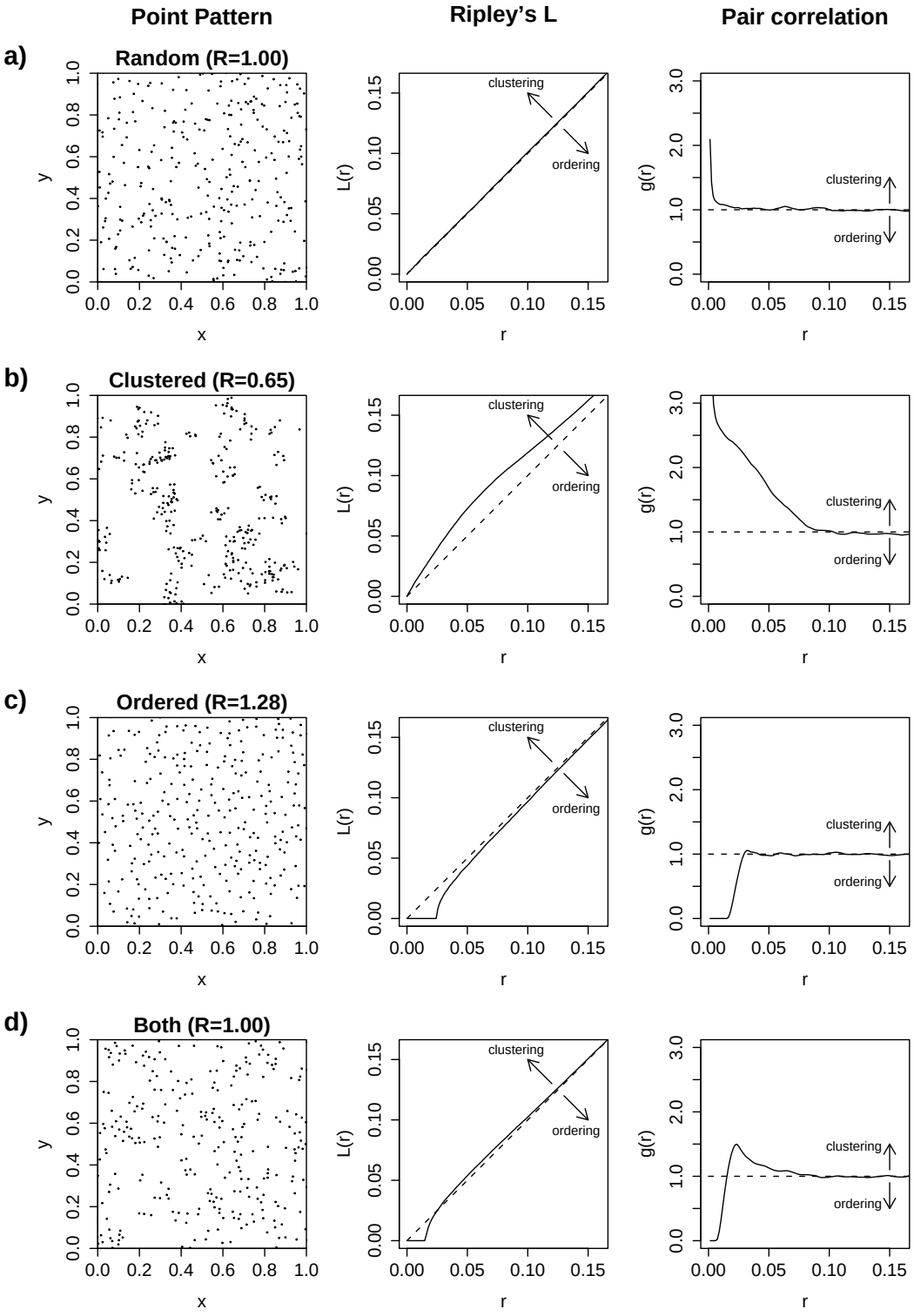

Fig. 1: Four example point patterns, with estimates of the aggregation index R, Ripley's $L(r)$ and the pair correlation function $g(r)$. Dashed lines show the behaviour expected for complete spatial randomness. The point patterns were generated by the following models: a) Complete spatial randomness; b) Neyman-Scott process (shows clustering); c) Hard core Strauss process (shows ordering); d) a different Neyman-Scott process, additionally thinned by removal of points closer than a particular distance (shows small scale ordering, large scale clustering).

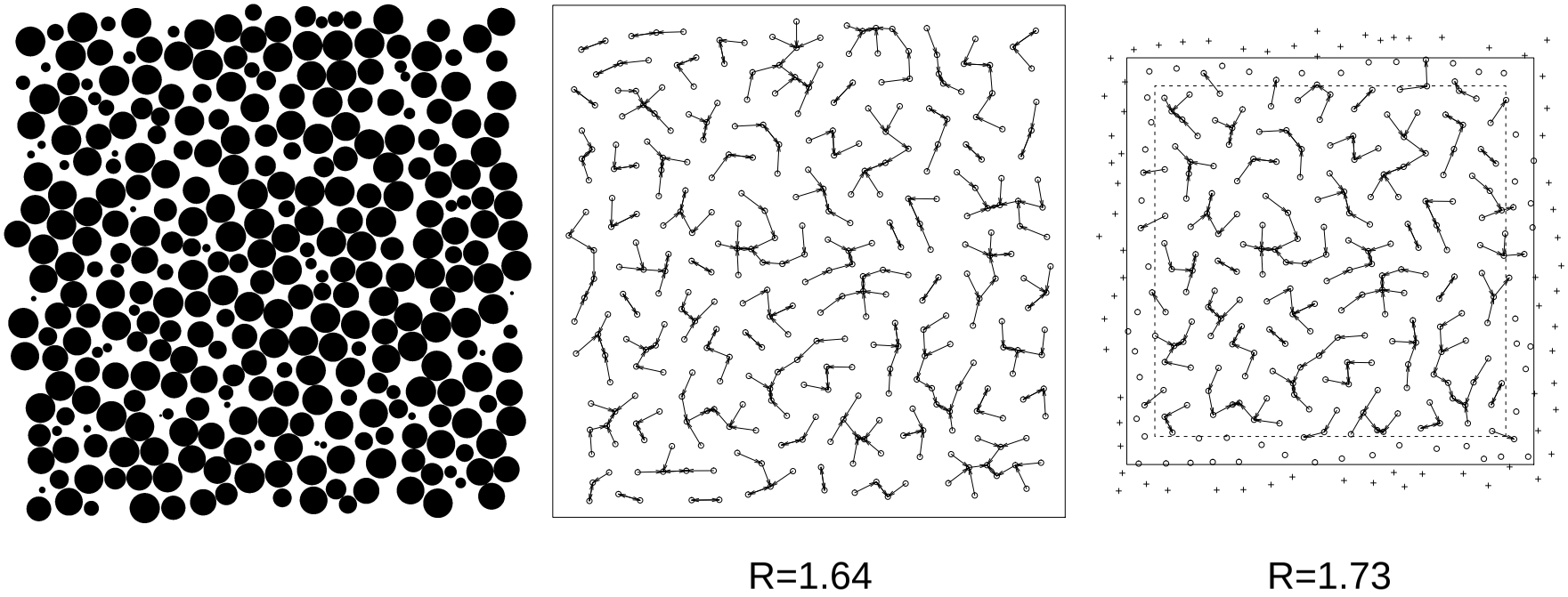

Fig. 2: An example of edge effects. Left figure shows a slice through a experimental random close packing of spheres by Finney (1970) (as used by Jerram et al. (1996)). Middle figure shows the point pattern generated by the centroids, with observation window (solid line) the same as that enclosing the original image. Arrows between points indicate their nearest neighbour. Right figure is the same point pattern, but with a smaller observation window, points outside of which are completely ignored. In calculating the mean nearest neighbour, only those points within the dashed box are considered, although the nearest neighbours are allowed to be found outside this dashed region. All points within the solid box are used for estimating the intensity.

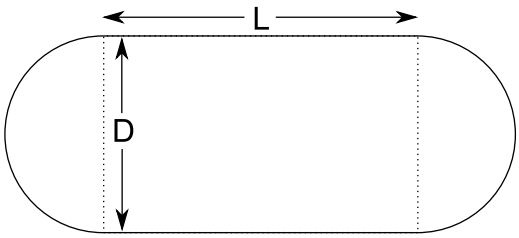

Fig. 3: Cross-section through a spherocylinder along its symmetry axis. $\alpha = L/D$.

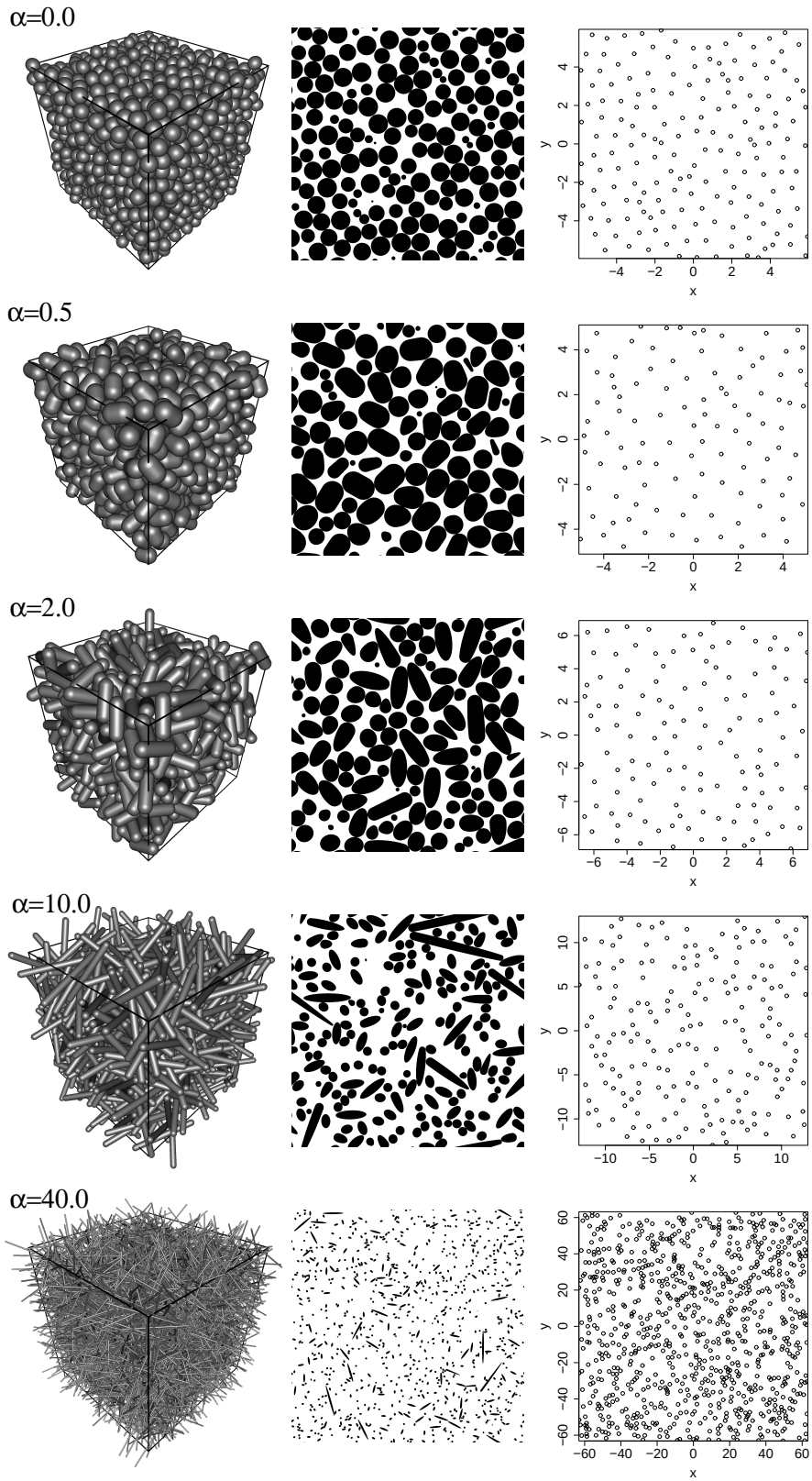

Fig. 4: Random close packings of spherocylinders for $\alpha = 0.0, 0.5, 2.0, 10.0$ and 40.0. Left column, 3D plots, with box of periodicity shown. Middle column, representative 2D slices. Right column, point patterns generated by the centroids of the 2D slices.

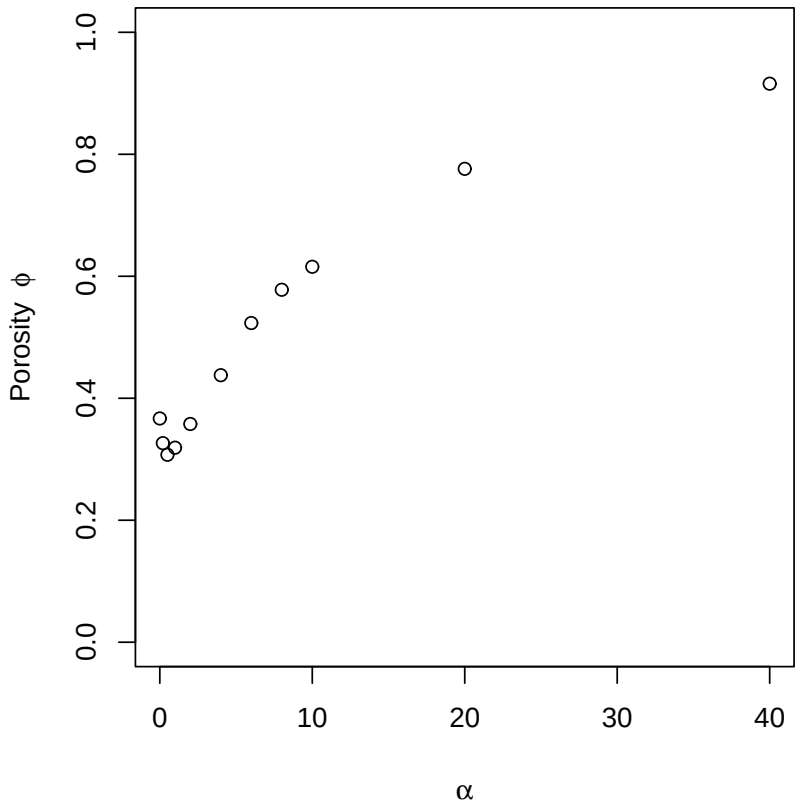

Fig. 5: Plot of porosity ϕ against α for random close packings of spherocylinders (based on Fig. 2 of Williams and Philipse (2003)).

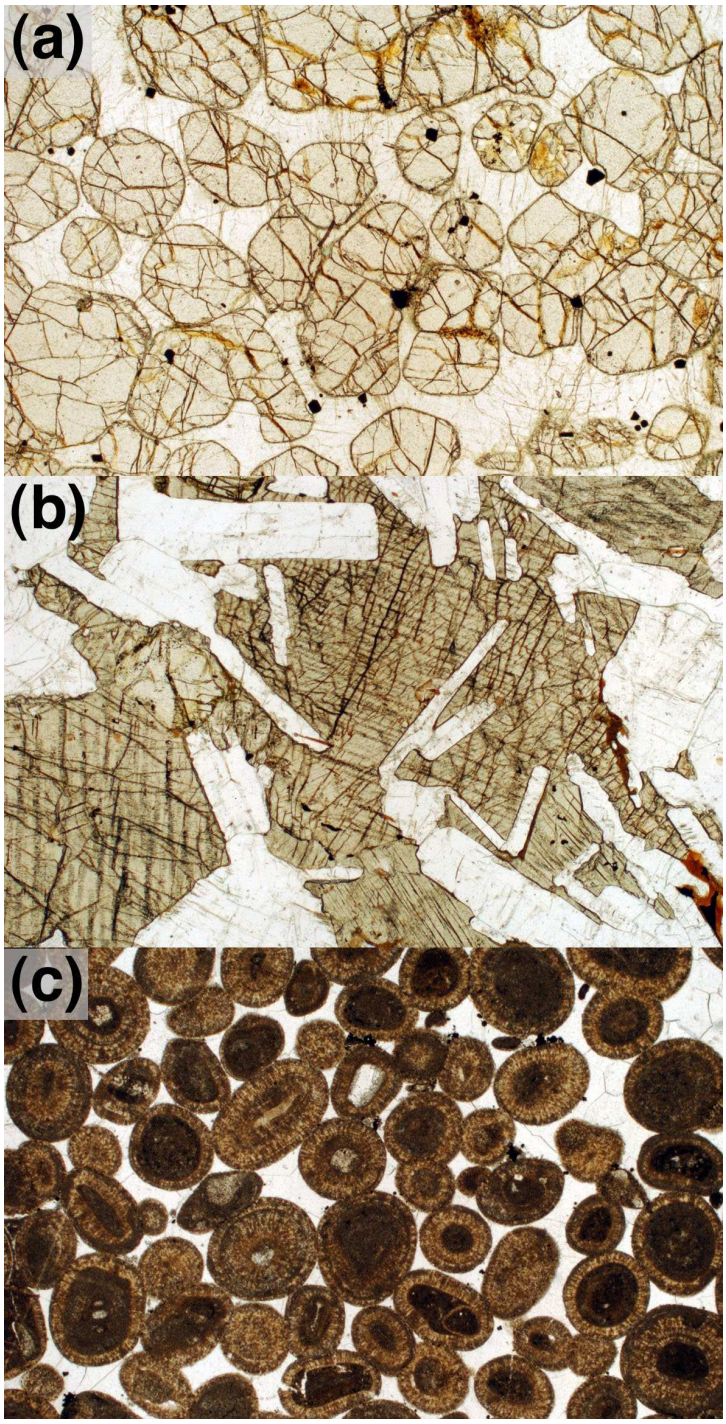

Fig. 6: Photomicrographs of thin sections under plane polarised light. The lower margin of each image is 4.5 mm long. (a) Olivine cumulate from the Eastern Layered Suite, Isle of Rum, in which rounded grains of olivine (with occasional small opaque grains of Cr-spinel) are enclosed by interstitial plagioclase. There is no evidence of compaction, although adjacent olivine grains have recrystallised to form mutual grain boundaries. (b) A polydisperse population of randomly oriented, framework-forming, elongate plagioclase primocrysts enclosed by a later-crystallising clinopyroxene oikocryst. This sample comes from the lower part of the Skaergaard Layered Series, where olivine and plagioclase were the only liquidus phases. (c) Oolitic limestone comprising a polydisperse population of rounded ooids enclosed by coarsely crystalline calcite cement.

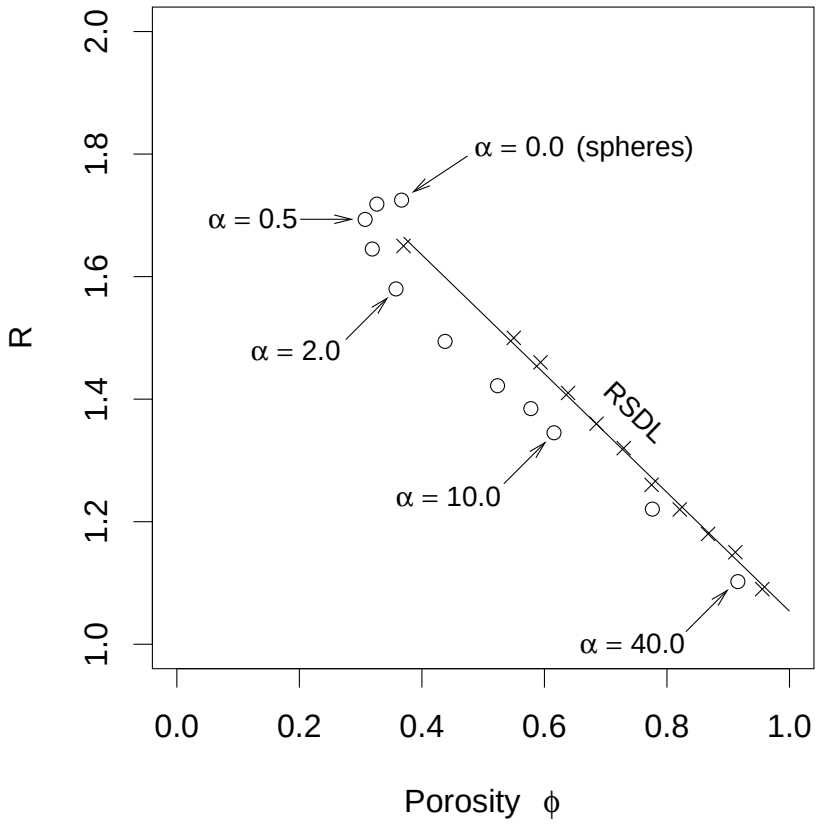

Fig. 7: Plot of aggregation index R against porosity ϕ (after Jerram et al. (1996)). Circles show points for random close packings of spherocylinders with $\alpha = 0.0$, 0.2, 0.5, 1.0, 2.0, 4.0, 6.0, 8.0, 10.0, 20.0, 40.0. The "Random Sphere Distribution Line" (RSDL) of Jerram et al. (1996) is also shown. Crosses show the numerical and experimental simulations of sphere packing used by Jerram et al. (1996) to define the RSDL.

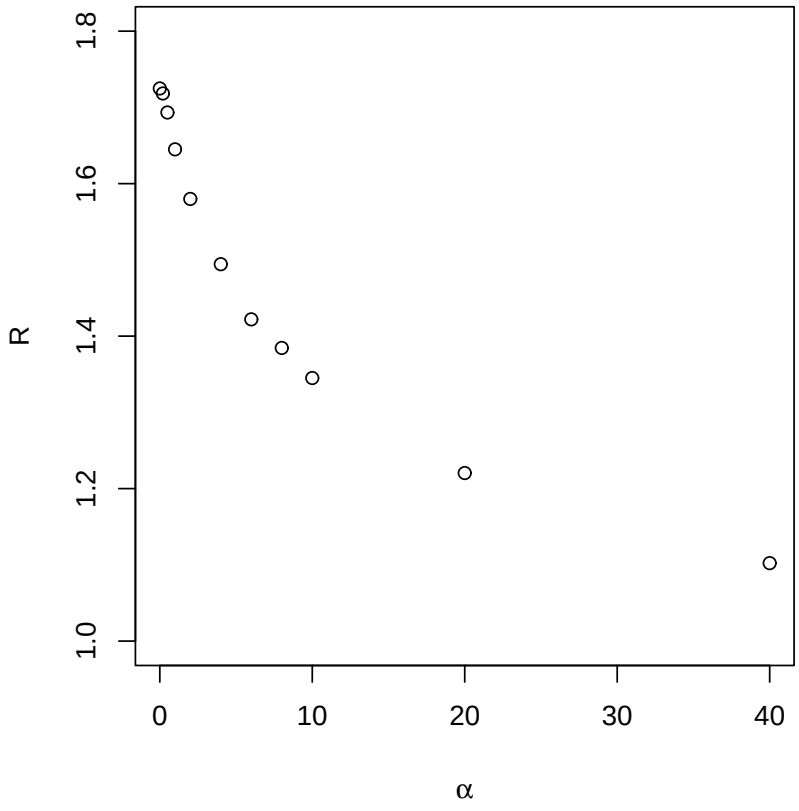

Fig. 8: Plot of aggregation index R against α for random close packings of spherocylinders.

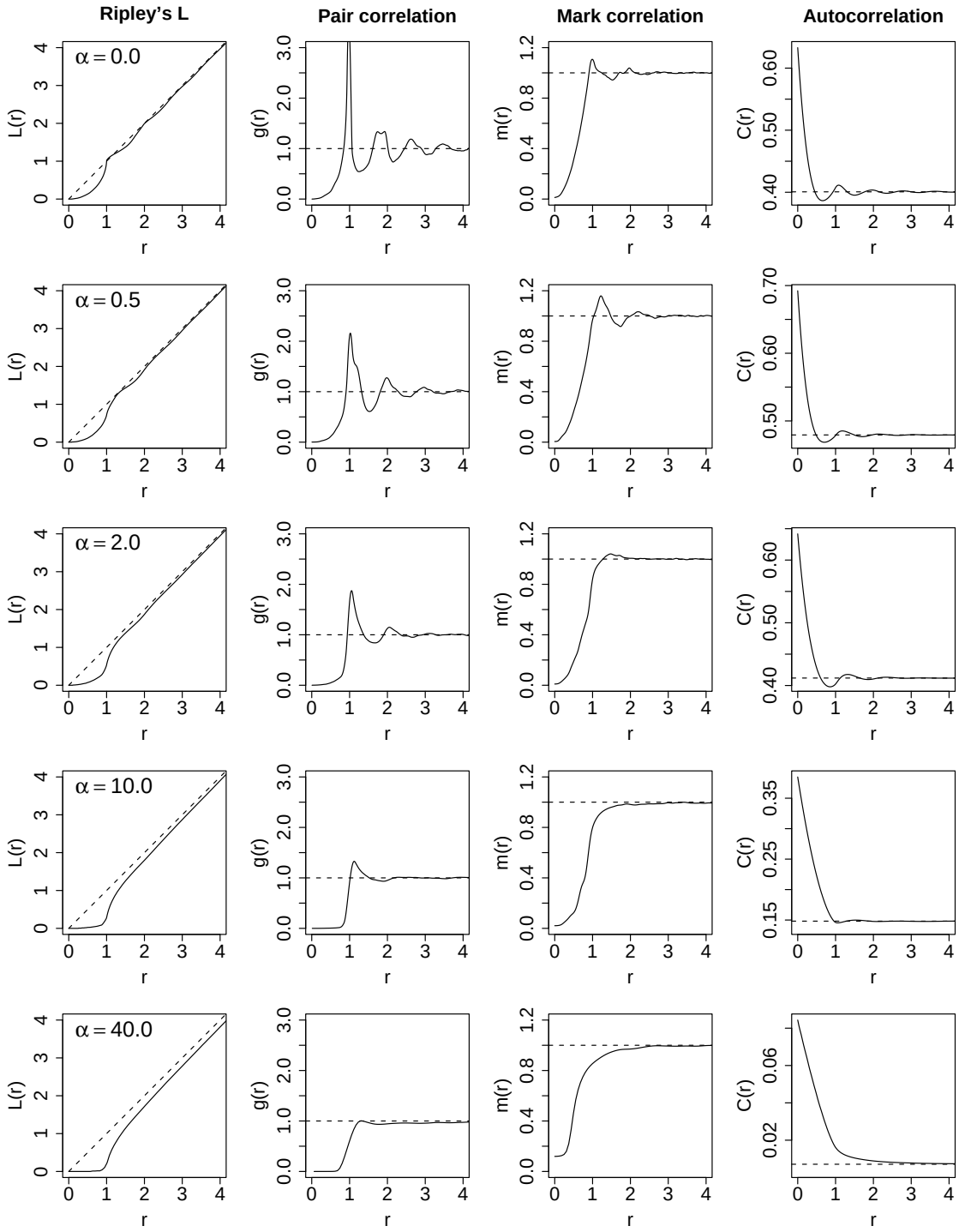

Fig. 9: Summary 2D thin section statistics for the random close packings shown in Fig. 4. First column, Ripley's $L(r)$. Second column, pair correlation function $g(r)$. Third column, mark correlation function $m(r)$, where marks are the effective radius of each grain cross-section. Fourth column, autocorrelation function $C(r)$. Units of distance are such that the diameter D of the spherocylinders is 1.

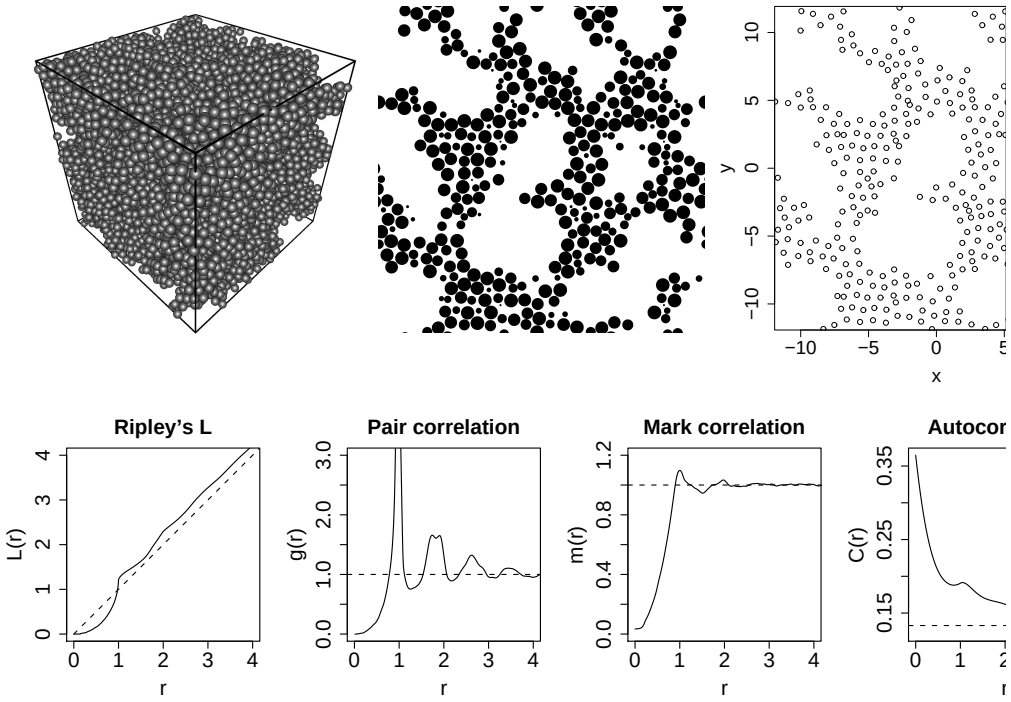

Fig. 10: An artificially clustered sphere texture (c.f. Fig. 6B of Jerram et al. 1996). $R = 1.36$, $\phi = 0.63$.

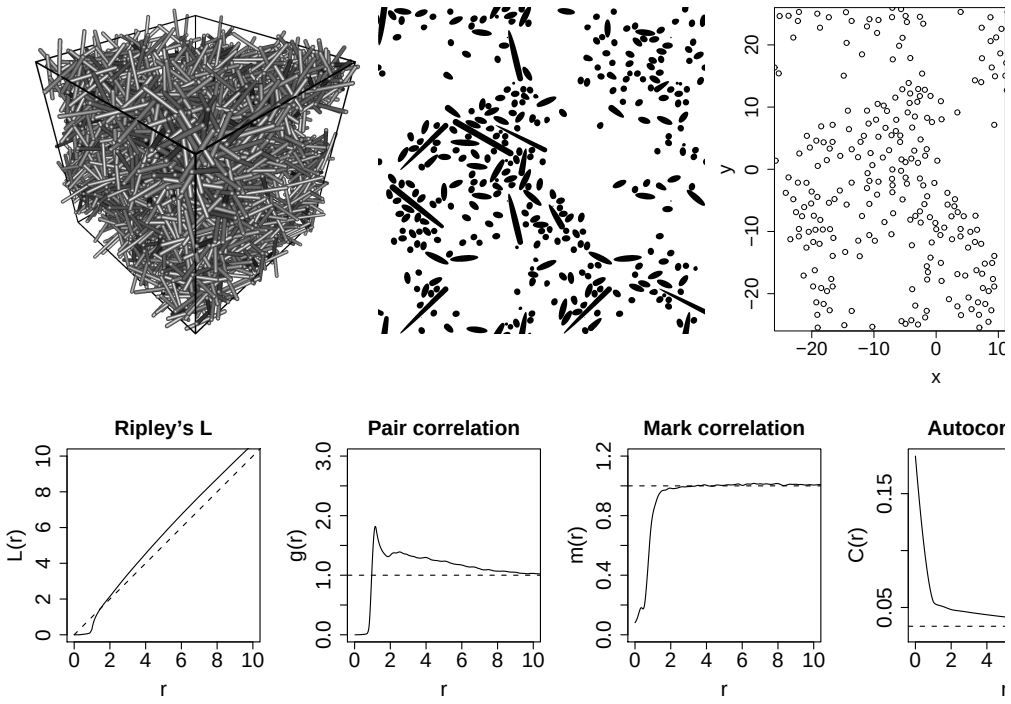

Fig. 11: An artificially clustered spherocylinder texture ($\alpha = 10.0$). $R = 1.07$, $\phi = 0.82$.

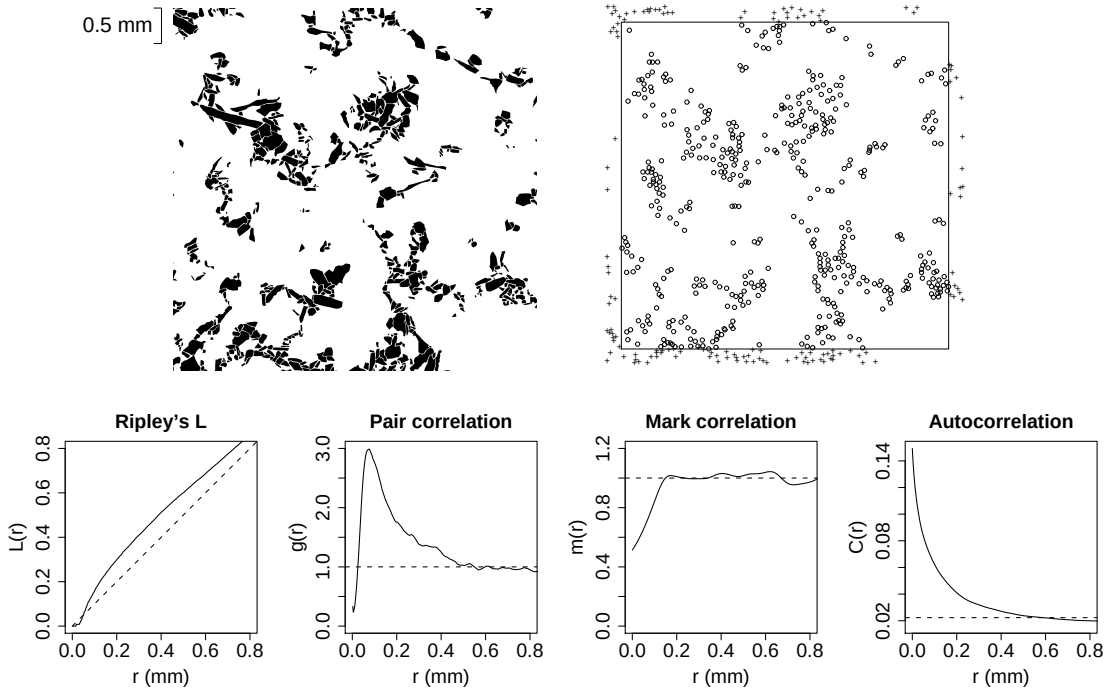

Fig. 12: A thin section from the Holyoake colonnade basalt (courtesy of D. Jerram). Image scale is 5 mm $\times$ 5 mm. Image shows plagioclase grains only. Point pattern statistics were calculated using an indented window as shown, to avoid edge effects due to incomplete grains. $R = 0.75$, $\phi = 0.85$.

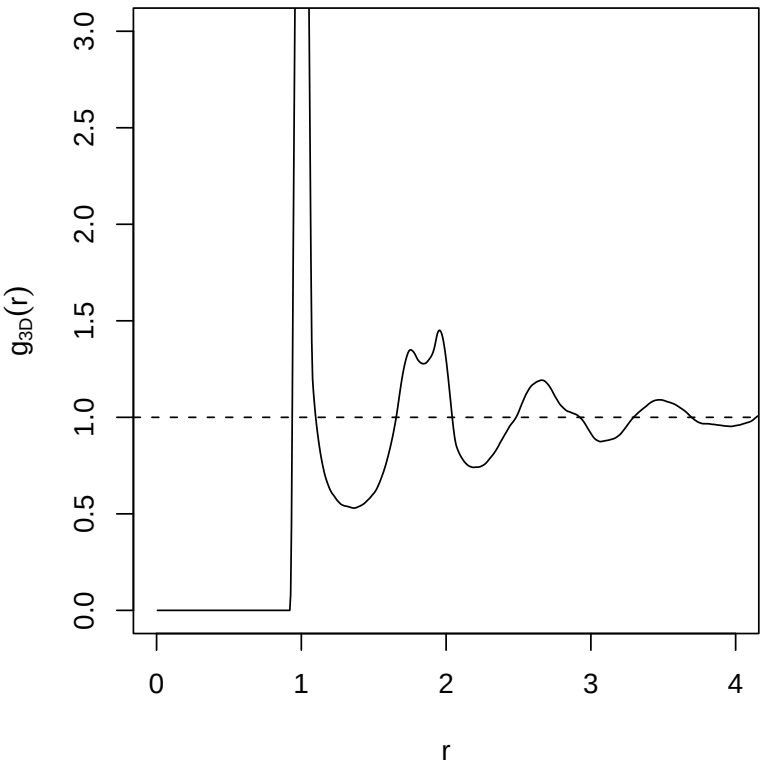

Fig. 13: The 3D pair correlation function of sphere centres for the random packing of spheres shown in Fig. 4 (see also Fig. 5 of Finney 1970, Fig. 7 of Wouterse and Philipse 2006, and Fig. 13 of Aste et al. 2005).